Kapal: Jurnal Ilmu Pengetahuan dan Teknologi Kelautan
(Kapal: Journal of Marine Science and Technology)

2301-9069 (e)
1829-8370 (p)

journal homepage : http://ejournal.undip.ac.id/index.php/kapal

# Comparative Analysis of Taper and Taperless Blade Design for Ocean Wind Turbines in Ciheras Coastline, West Java

Madi[1)*], Tuswan[2)], Ilham Dwi Arirohman[1)], Abdi Ismail[2)]

[1)] Energy System Engineering, Institut Teknologi Sumatera, South Lampung 35365, Indonesia
[2)] Department of Naval Architecture, Institut Teknologi Sepuluh Nopember, Surabaya 60111, Indonesia
[*)] Corresponding Author : madi@tse.itera.ac.id

**Article Info**

**Keywords:**
Taper blade,
Taperless blade,
Ocean wind turbine,
Ciheras Coastline,
NACA 4412,

**Article history:**
Received: 27/08/20
Last revised: 11/11/20
Accepted: 13/11/20
Available online: 13/11/20
Published: 28/02/21

**DOI:**
https://doi.org/10.14710/kapal.v18i1.32486

**Abstract**

The blade is the most critical part of turbine design because it is used to convert kinetic to mechanical energy. In general, the blade types used for ocean wind turbines are taper and taperless blades, like those operated at Ciheras Coastline. Previous research has been analyzed the type of airfoil used in designing taper blades for ocean wind turbines using NACA 4412, which was selected as the optimal foil configuration at sea wind speeds of 12 m/s. In this study, the comparison of taper and taperless blade designs using NACA 4412 at a wind speed of 12 m/s is analyzed. The comparative study with previous research has been carried out and resulted in the same graphical patterns and performance results. In this study, the focus is on investigating the performance coefficient of power, mechanical power, and electrical power. The final result shows that taper blade designs are highly recommended for use in ocean wind turbines compared to taperless blades. In general, the performance produced by taper blades is more significant than taperless blades at relatively high wind speeds. The maximum performance coefficient of power, mechanical power, and electrical power generated by the taper blades in sequent are 0.47, 1535 watts, and 786 watts, while the taperless blades have 0.44, 1437 watts, and 736 watts.



## 1. Introduction

Turbines are one of the leading technologies used for generating electricity other than generators [1]. In general, there are two types of turbines based on the rotating axis, such as vertical and horizontal turbines. The horizontal axis turbine is more commonly used for the development of wind power plants with a research and development percentage of 43%, while the vertical turbine is about 33% [2]. Based on the efficiency produced by the turbine value (Cp), the horizontal type provides a higher Cp than the vertical type. In general, the Cp value of the horizontal turbine is above 0.4 (40%), while the vertical turbine is above 0.3 (30%) [3].

In designing a horizontal turbine, it will not be separated to develop the blades because it is the main component that can convert kinetic energy into mechanical energy. In general, the types of blades consist of taper, taperless, and inverse taper blades. The tapered blade has a tip smaller than the base, the taperless blade has a similar size of the tip and the base, while the inverse taper has a bigger tip than the base [4]. The illustration of each type of blade can be shown in Figure 1.

Airfoil, as the basic form of the blade, has been developed by several researchers. A new type of airfoil was designed from low Reynolds number airfoils based on their aerodynamic performance [5]. The Seagull Airfoil has been developed using the results of a foreign bionic experimental airfoil. This investigation showed that the seagull airfoil was suitable for small-scale horizontal wind turbines [6]. The blade design has been developed from a combination of two airfoils FX66-S-196 and NACA63-621 [7,8]. The 3 kW horizontal wind turbine has been developed using the NACA 4418 [9].

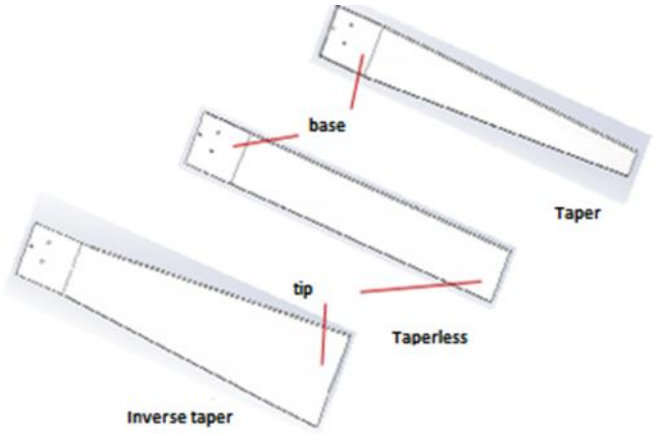


Figure 1. Type of Blades in Horizontal Axis Turbine

Airfoil characteristics are studied to be applied to horizontal wind turbines experimentally. Experimental studies have been carried out on the thin airfoil SG series thin airfoils (SG6040 – SG6043) for small-scale wind turbines [10]. Experimentally, the AF300 airfoil was tested in the wind tunnel to compare the performance of 8 other airfoils [11]. Besides the airfoil aspect, the yaw characteristic of the horizontal wind turbine has also been analyzed experimentally using a model with a diameter of 1 m [12]. The horizontal wind turbine has been installed, and its performance has been analyzed in several locations around Nepal [13].

Experimental studies require relatively more expensive costs so that analytical methods and numerical methods are developed to determine airfoil performance, where the most popular method used is the blade element momentum (BEM) method. The blade element momentum (BEM) method has been developed to design a 1 kW horizontal wind turbine using an SD 7062 airfoil [14]. Aerodynamic analysis using the blade element momentum (BEM) method has been carried out on the blade of the small-scale horizontal axis wind turbine [15]. Comparative studies have been carried out on aerodynamics performances of the BEMT-blade and the Baseline-blade, a non-twisted and non-tapered type [16].

Yaw characteristic of the horizontal wind turbine can also be developed using a theoretical equation [17]. Moreover, the starting characteristic of the horizontal wind turbine has been investigated using the classical blade element theory and wake modelling. Blade pitch angles between 0° and 35° have been analyzed to determine the starting characteristic of the horizontal wind turbine [18]. Numerical studies have been carried out to determine the lift and drag characteristic of the NACA0018 wind turbine airfoil [19]. Rocha et al. [20] conducted a computational analysis on a small-scale horizontal axis wind turbine using the SST k–ω turbulence model. Furthermore, Edge Element-Momentum and Computational-Fluid-Dynamics analysis was carried out on the blended airfoil of a horizontal wind turbine [21].

Numerical studies have major constraints on the availability of software licenses. Open-source software for performing aerodynamics analysis on horizontal wind turbines, such as the open-source Q-Blade software, can be a solution. In addition, developing countries need applied research in specific locations, using easy-to-build airfoils, and supported by open-source software for wind turbine analysis. Wind turbine operation in Indonesia has been implemented on the Ciheras coastline operated by PT. Lentera Angin Nusantara. In general, the types of blades used are taper and taperless blades. Successful research by PT. Lentera Angin Nusantara to build a wind turbine can trigger and motivate young Indonesian researchers to study the potential of wind energy development, especially in Indonesia's ocean area. Previous research has analyzed the design of taper blades for ocean wind turbines at Ciheras coastline by PT. Lentera Angin Nusantara. The focus of the study investigated the type of foil, such as Clark-Y, NACA 4412, NACA 3612, NACA 4418, NACA 0012, and NACA 0018. The final results show that NACA 4412 has the best performance at sea wind speeds of 12 m/s [22]. Moreover, NACA 4412 is also relatively easy-to-make. So, further research needs to be conducted to investigate the performance of NACA 4412 foil with different blade configuration types.

Apart from selecting the type of foil used on the blades, it is also necessary to choose the number of blades because it greatly determines the performance of a turbine. The research on the number of blades has been carried out, and the optimal results are three blades compared two blades and four blades [23]. Based on the previous work, this research will focus on investigating the performance of three blades for ocean wind turbines.

The location chosen in this study is on Ciheras Coastline, which is one of the southern coasts of Java Island, as shown in Figure 2. The potential for wind on Ciheras Coastline is suitable to be used to drive a power generator turbine, with an average wind speed of 3-12 m/s. The wind speed that has the potential to turn the turbine must be above 5 m/s and can be found in most place on the south coast of Java Island [24]. Thus, Ciheras Coastline, which is the centre of wind turbine studies by PT. Lentera Angin Nusantara is very suitable to be used as a research location for new and renewable energy sourced from the ocean wind.

The objective of the research is to analyze the performance comparison of different blade types. Two different blade types, such as taper and taperless blades are compared by analyzing the performance and power of the blade using the open-source software Q-Blade in Ciheras Coastline, West Java. The results of this study are expected to be used as a reference for other researchers to study developing marine wind turbine technology in Indonesia. as we know, given the huge potential of sea breezes in Indonesia, but until now it has not been optimally utilized for future energy. In addition, the results of this preliminary study can be used as recommendations for supporting methods such as Computational Fluids Dynamics (CFD), Experimental Fluids Dynamics (EFD), and field studies of marine wind turbine models.


Figure 2. The Wind Turbine in Ciheras Coastline, West Java

## 2. Methods

### 2.1. Turbine Blade Geometry

The design of taper and taperless blade marine wind turbines can be shown in Figure 3. The taper blade has a tip smaller than the base, the taperless blade has a similar size of the tip and the base, while the inverse taper has a bigger tip than the base. Meanwhile, the turbine blade geometry data refers to the research conducted by Madi et al. [22], which can be shown in Table 1.

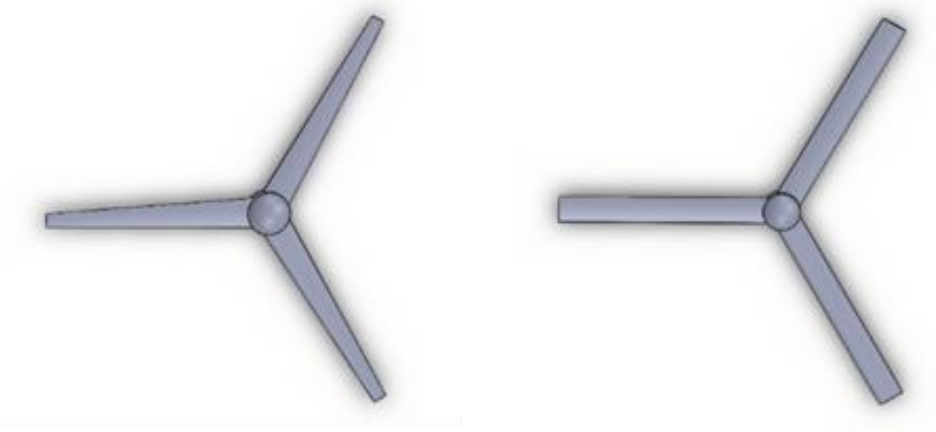

(a) (b)

Figure 3. Blade Types, (a) Taper, and (b) Taperless

Table 1. Turbine Blade Geometries NACA 4412

| Parameters | Value |
|---|---|
| Number of blades | 3 |
| Blades length | 1 m |
| Hub radius | 0.22 m |
| Number of blades element | 10 |
| Ocean wind speed | 12 m/s |

### 2.2. Performance Parameters

In determining the performance of turbine blades, this study uses only the analytical method with Q-Blade software. Q-Blade uses Euler-Bernoulli Beam Module. The foil profile of the blade is analyzed using the Q-Blade in the range of angle of attack -5° to 50° with Reynold numbers 100000. After that, the Q-Blade software will give the results of the lift coefficient ($C_l$) against the angle of attack ($AoA$). The turbine blade geometry is formed using the Q-Blade by providing position, chord, and twist input values. After that, it is analyzed for a tip speed ratio $TSR$ ($\lambda_r$) of 1 to 10, a wind density of 1.225 kg/m$^3$, and a viscosity of 0.0000178 kg/ms, and then the Q-Blade gives the results of power coefficient ($C_p$) on $TSR$. As for getting the position, chord, and twist values using the following parameter equation; the first parameter needed is to calculate the position of the blade element ($r$) using the following equation [25].

$$r = 0.22 + \left[\left(\frac{R - 0.22}{n}\right) x\ element\right] \quad (1)$$

where $R$ is the length of the blade in meters (m) and $n$ is the number of blade elements. The second parameter needed is to calculate the partial $TSR$ ($\lambda r$) of each blade element by using the following equation [25].

$$\lambda_r = \frac{r}{R}\ x\ \lambda_R \quad (2)$$

where $\lambda_R$ is the $TSR$ that has been determined for the calculation, which is assumed as 7 The third parameter needed is to calculate the chord width ($C_r$) for each blade element by calculating using the following equation [25].

$$C_r = \frac{16\pi\ x\ R\ x\ \frac{R}{r}}{9\lambda^2\ x\ B\ x\ C_l} \quad (3)$$

where $C_l$ is the lift coefficient obtained from the design results, and $B$ is the number of blades. The fourth parameter is to calculate the flow angle ($\phi$) for each blade element using the following equation [25].

$$\phi\ = \frac{2}{3} tan^{-1} \frac{1}{\lambda_r} \quad (4)$$

The fifth parameter is the twist angle ($ß$) on each blade element, using the following equation [25].

$$\beta\ = \phi - \alpha \quad (5)$$

where $\alpha$ is the angle of attack is $6^0$ obtained from the design results. These five parameters are taken into account to design the taper and taperless blade shapes. The parameters needed to determine the performance of the blades are, first by calculating the wind kinetic power ($P_a$), using the following equation [25].

$$Pa\ =\ 0{,}5\ p\ A\ V^3 \quad (6)$$

where $p$ is the density of the wind, which is 1.225 kg/m$^3$, $A$ is the turbine swept area (m$^2$), and $V$ is the ocean wind speed (m/s). Besides that, calculating for the performance of turbine mechanical power ($P_t$) using the following equation [25].

$$P_t\ =\ C_p\ x\ P_a \quad (7)$$

where $C_p$ is a power coefficient. It is obtained from the design result. The last performance is calculating the amount of electric power ($P_l$) generated, using the following equation [25].

$$P_l\ =\ \eta_{sys}\ x\ P_a \quad (8)$$

where, $\eta_{sys}$ is the system efficiency from the multiplication of blade efficiency ($C_p$), generator efficiency (80%), controller (80%), and transmission (80%).

## 3. Results and Discussion

### 3.1. Comparative Assessment

The comparison in this research is to compare the performance with previous studies. The $C_p$ obtained from the simulation results using the open-source software Q-Blade v.08. The data used are the same as in previous studies. This research uses the method of analysis with a structural Euler-Bernoulli beam module on Q-Blade software. The results are in the value of $TSR$ and $C_p$ curves, as shown in Figure 4. The figure shows a similar value of $TSR$ and $C_p$ between the results of the study and the previous data. The red curve is the result of the performance of the previous study [22], while the blue curve is the result of the performance of this study. The $TSR$ ranges used are from 1 to 10. The $TSR$ that is capable of resulting $C_{Pmax}$ on both graphs is the same ($TSR$ = 7) according to the initial design.

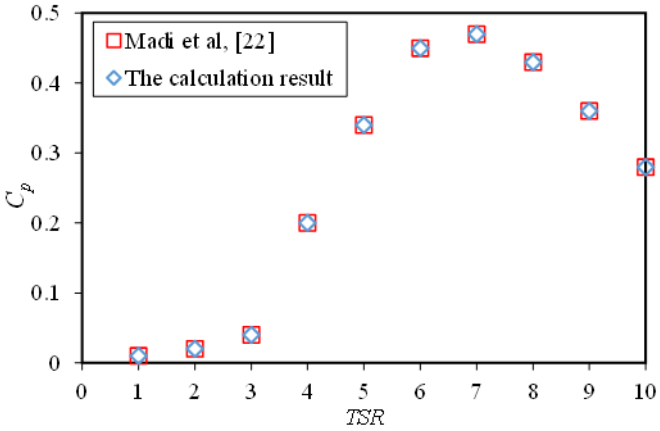


Figure 4. Comparative Assessment with Previous Research

Figure 4 shows that $C_p$ value is very low below 0.1 at *TSR* 1 to 3. It is caused by *TSR* represents the value of sea wind speed, so that at low *TSR* the sea wind speed is also low. Based on Eq. 6, if the sea wind speed is low, the sea wind kinetic power value is low too. As a result, $C_p$ generated by the turbine blades becomes very small based on Eq. 7, When *TSR* 4 shows $C_p$ results increase sharply to the maximum point on *TSR* 7. The sea breeze increases until the maximum sea wind speed of 12 m/s on *TSR* 7 with a maximum $C_p$ value of 0.47. This event is usually called a pre-stall, an event towards the peak point before a stall occurs. At *TSR* 8 to 10, the results have shown a stall event which causes $C_p$ value decreases after reaching its maximum point. The possibility of a stall occurs because the turbine blade is unable to maintain the lift force after reaching equilibrium at the maximum $C_p$.

### 3.2. Comparison of Taper and Taperless Blade Geometry Design

The geometry of the taper blade (position, chord, and twist) used in this study is the same as the previous study [22]. This study compares the results with another type of blade, namely taperless blade to determine the best performance of the two types of blades that are feasible used for marine wind turbines. The geometry is obtained based on calculations using Eq. 1 to Eq. 5.

Based on Eq. 1, the partial radius values for the taper and taperless blades are obtained. The partial radius on each element of the taper and taperless blades are the same. It is caused by the same hub position of both types ($r$ = 0.22 m) and the same blade length, which is 1 m. So, the calculation of the same partial radius is obtained for each element. The partial radius or position of the taper and taperless blade positions on elements 1 to 10 are 0.30 m, 0.38 m, 0.45 m, 0.53 m, 0.61 m, 0.69 m, 0.77 m, 0.84 m, 0.92 m, and 1 m.

Based on Eq. 2 and Eq. 3, partial *TSR* values and partial chord length ($C_r$) are obtained on the taper and taperless blades, as shown in Table 2. The table has shown that the partial *TSR* values for the taper and taperless blades are the same because the values for the partial radius ($r$) on the two blades are also the same. Meanwhile, the chord length value ($C_r$) shows different results for the two types of blades. On the taper bar starting from elements 0 to 10, the $C_r$ value is getting smaller.

As a result, the tip of the taper blade design is smaller than the base. Meanwhile, the taperless blade elements show the same amount of $C_r$. It means that the tip design of the taperless blade is as large as the shape of the base. Based on Eq. 4 and Eq. 5, the partial *TSR* and chord length ($C_r$) values were obtained on the taper and taperless blades, as shown in Table 3. The table has shown that the values of $\phi$ and $ß$ for both blade types are the same because the partial *TSR* values based on the calculation result show the same values as well. The process of linearizing $ß$ and $C_r$ data is needed to determine the shape of the design of the two types of blades. The $ß$ and $C_r$ linearization data on the taper and taperless blades can be shown in Table 4.

Table 2. Comparison of $\lambda_r$ and Chord Length ($C_r$) of the Taper and Taperless Blade Element

| Number of element | Taper Blade | | Taperless Blade | |
|---|---|---|---|---|
| | *TSR* ( $\lambda_r$ ) | $C_r$ (m) | *TSR* ( $\lambda_r$ ) | $C_r$ (m) |
| 0 | 1.54 | 0.15 | 1.54 | 0.15 |
| 1 | 2.09 | 0.11 | 2.09 | 0.15 |
| 2 | 2.63 | 0.09 | 2.63 | 0.15 |
| 3 | 3.18 | 0.07 | 3.18 | 0.15 |
| 4 | 3.72 | 0.06 | 3.72 | 0.15 |
| 5 | 4.27 | 0.06 | 4.27 | 0.15 |
| 6 | 4.82 | 0.05 | 4.82 | 0.15 |
| 7 | 5.36 | 0.04 | 5.36 | 0.15 |
| 8 | 5.91 | 0.04 | 5.91 | 0.15 |
| 9 | 6.45 | 0.04 | 6.45 | 0.15 |
| 10 | 7.00 | 0.03 | 7.00 | 0.15 |

Table 3. The Value of $\phi$ and $ß$ of the Taper and Taperless Blade Element

| Number of element | Taper Blade | | Taperless Blade | |
|---|---|---|---|---|
| | $\phi$ | $ß$ | $\phi$ | $ß$ |
| 0 | 22.00 | 16.00 | 22.00 | 16.00 |
| 1 | 17.07 | 11.07 | 17.07 | 11.07 |
| 2 | 13.87 | 7.87 | 13.87 | 7.87 |
| 3 | 11.64 | 5.64 | 11.64 | 5.64 |
| 4 | 10.02 | 4.02 | 10.02 | 4.02 |
| 5 | 8.79 | 2.79 | 8.79 | 2.79 |
| 6 | 7.82 | 1.82 | 7.82 | 1.82 |
| 7 | 7.04 | 1.04 | 7.04 | 1.04 |
| 8 | 6.40 | 0.4 | 6.40 | 0.4 |
| 9 | 5.87 | -0.13 | 5.87 | -0.13 |
| 10 | 5.42 | -0.58 | 5.42 | -0.58 |

Table 4. Linearization of $ß$ and $C_r$ of the taper and taperless blade element

| The radius of the taper blade ($r$) | Taper Blade | | Taperless Blade | |
|---|---|---|---|---|
| | Linearization of $ß$ | Linearization of $C_r$ | Linearization of $ß$ | Linearization of $C_r$ |
| 0.22 | 5.66 | 0.07 | 5.42 | 0.15 |
| 0.30 | 5.00 | 0.07 | 4.79 | 0.15 |
| 0.38 | 4.34 | 0.07 | 4.17 | 0.15 |
| 0.45 | 3.69 | 0.06 | 3.54 | 0.15 |
| 0.53 | 3.03 | 0.06 | 2.92 | 0.15 |
| 0.61 | 2.37 | 0.05 | 2.29 | 0.15 |
| 0.69 | 1.71 | 0.05 | 1.66 | 0.15 |
| 0.77 | 1.05 | 0.04 | 1.04 | 0.15 |
| 0.84 | 0.40 | 0.04 | 0.41 | 0.15 |
| 0.92 | -0.26 | 0.04 | -0.22 | 0.15 |
| 1.00 | -0.92 | 0.03 | -0.84 | 0.15 |

Based on the calculation of the parameters, the taper blade shape is shown in Figure 5a, and the taperless blade is shown in Figure 5b. The first one shows that the blue line is the $C_r$ - $r$ curve, which is the $C_r$ data before being linearized. The yellow line is the $C_r$ data after being linearized, and the red line is the 25% $C_r$ data linearization to form the taper bar. So that in Figure 5, two lines form the taper blade, such as the yellow and red lines. Figure 5b shows that the blue line is the $C_r$ - $r$ curve, which is the $C_r$ data before being linearized. The red line is the $C_r$ data after 25% linearization to form a taperless blade. Thus, two lines form the taperless blade, which is blue and yellow lines.

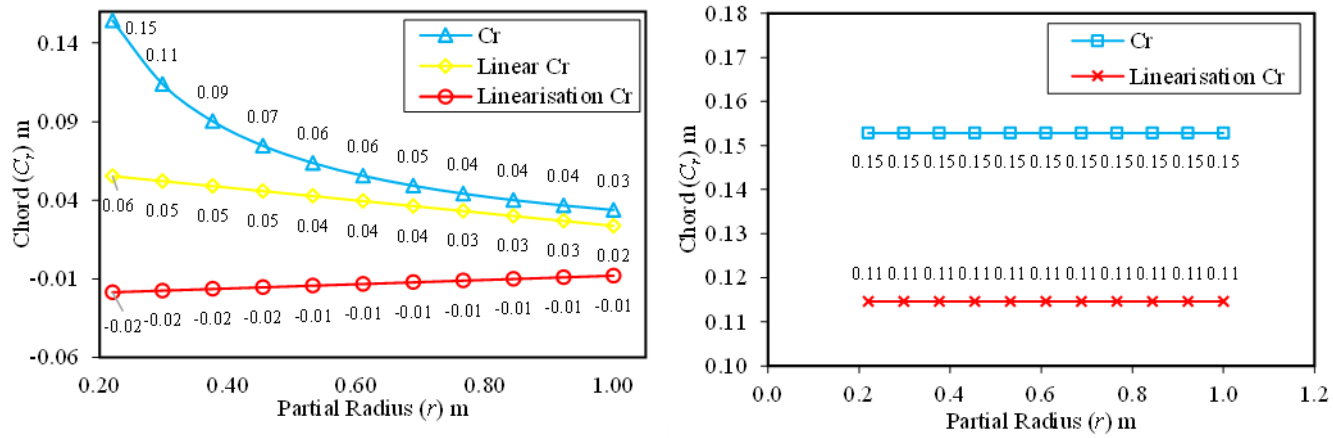


(a) (b)

Figure 5. The Relation Between Partial Radius ($r$) and Chord Length ($Cr$) a) Taper b) Taperless

### 3.3. Comparison of Taper and Taperless Blade Geometry Design

The blade performance referred to in this study is the lift coefficient ($C_l$), the torque coefficient ($C_T$), and the power coefficient ($C_p$). These three performances are obtained by using the method of analysis with a structural Euler-Bernoulli beam module on the Q-Blade software. $C_p$ taper blade in this study has been compared with previous research [22], as described in Figure 4. $C_p$ value represents the $C_l$ and $C_T$ values to compare with previous studies [22]. It is caused by $C_p$ is the

magnitude of the kinetic power of the sea breeze that can be absorbed by the turbine blades. If $C_p$ values in this study are comparable to those before [22], then $C_l$ and $C_T$ values will follow. Furthermore, this study adds another blade variation, namely the taperless blade compared to the taper blade that has been compared with previous studies [22].

The performance of a turbine that uses foil on the blades cannot be separated from the analysis of the lift force, which the lift that can trigger the turbine to rotate. Thus, the lift force is significant to determine the ability of the turbine to rotate. The lift force is represented by the lift coefficient ($C_l$). The lift coefficient is generally related to the angle of attack (*AoA*), which is the angle formed from the wind direction with the chord line. The $C_l$ -*AoA* results on taper and taperless blades can be shown in Figure 6. The figure shows the red line is the result of the lift coefficient on the taper blades, while the green line is the result of the lift coefficient on the taperless blades. As can be seen, the result explains that taperless blades produce a higher lift coefficient than taper blades. In conditions *AoA* 1 to 10, the two types of blades have shown very coinciding and increasing results. It means that under these conditions, the lift coefficient on the two blade types is in the pre-stall period

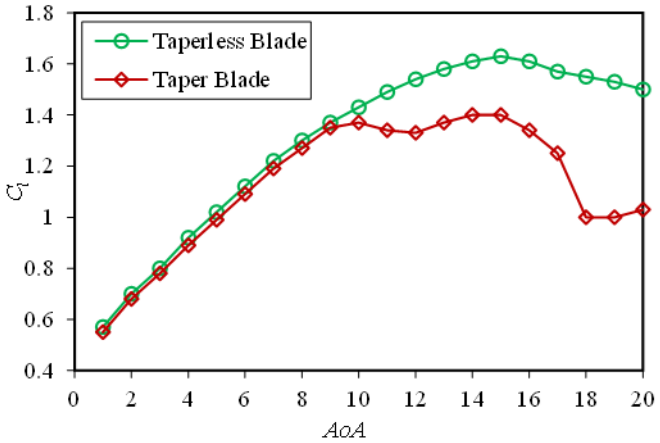


Figure 6. *Cl-AoA* Curve of Taper Blade and Taperless Blade

However, in this study, the taper blade shows a slight stall of the coefficient of lift which begins at *AoA* 10 to 11, then slightly increases and a larger stall occurs at *AoA* 17 to 18. The occurrence of a stall has happened when the lift coefficient performance has the maximum value. Then, the value will decrease as *AoA* increases. The stall of lift coefficient on the taperless blade occurs during *AoA* 16 to 17. The earlier stall occurs on the taper blade possibly due to the uneven distribution of the wind on the foil cross-section. It is caused by the unequal width of the foil and the smaller cross-section to the tip of the blade. However, after a stall, both blades maintain a stable lift coefficient. In general, the results of the lift coefficient on the two blades do not adequately describe a better performance because there are other factors such as the torque coefficient and the power coefficient.

The torque coefficient ($C_T$) is a dimensionless number that represents the magnitude of torque. In general, the $C_T$ curve is related to the type of speed ratio (*TSR*), which represents a dimensionless number that represents wind speed. The simulation results of this study have shown the $C_T$ -*TSR* curve, which can be seen in Figure 7. The red line curve is the $C_T$ result on the taper blade, while the green line is the result of the taperless blade. In the taper blade, there is an increase in $C_T$ from *TSR* 1 to 10, while the taperless blade increases $C_T$ from *TSR* 1 to 7, and after that, it shows stable results. It means that in the *TSR* range 1 to 10 there is a continuous increase in torque on the taper blades. Thus, at relatively high wind speed, it is very well recommended to use a taper blade design while the taperless blade design is excellent if used during low to moderate wind speed conditions. It is caused by the increase of torque stops at *TSR* 7. After that, it is stable, and the stall will possibly occur when the *TSR* is more than 10.

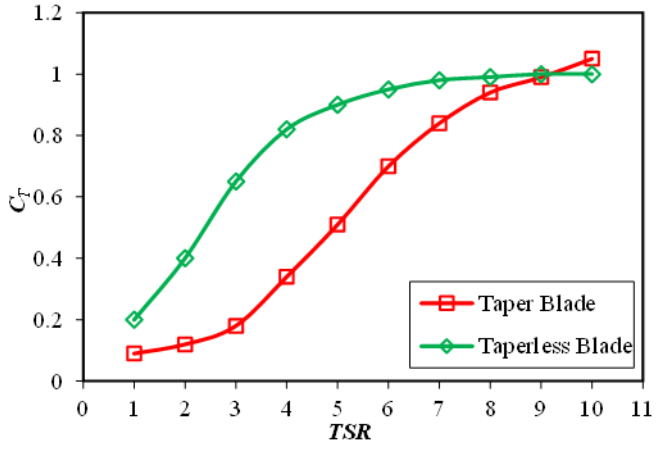


Figure 7. *TSR*- $C_T$ Curve of Taper and Taperless Blades

The power coefficient ($C_p$) is a dimensionless number that represents the magnitude of turbine power. In general, the $C_p$ curve is related to *TSR*. The simulation results of this study have shown $C_p$-*TSR* curve in Figure 8. The red line curve is the result of $C_p$ on the taper blade, while the green line is the result of the taperless blade. As can be seen in Figure 8, *TSR* 1 to 5 shows that the green curve is above the red curve.

On the contrary, it can be seen in *TSR* 6 to 10 that the red curve is above the green curve. From that result, it can be concluded that taperless blades show better mechanical power performance than taper blades during *TSR* 1 to 5. However, in *TSR* 6 to 10 taper blades show better mechanical power performance than taperless blades. Based on the study case, the results show that taper blades are able to provide better performance than taperless in high wind speed conditions. In this case, it can be said that taper blades are perfect for use as an ocean wind turbine design which is classified as high wind speed. For the taperless blade, it is not recommended using in high wind speed because a stall will occur and will decrease the performance. Its design can be applied to low to moderate wind speeds. As a result, taperless blades are not recommended for wind turbine blade design.

The $C_p$ -*TSR* curve of taper and taperless blades has shown in Figure 8. As can be seen in *TSR* 7, the taper blade yields the best performance with $C_p$ 0.47 (47%) compared to taperless with $C_p$ 0.39 (39%). It can be concluded that taper blade has better performance with $C_{pmax}$ 0.47 at *TSR* 7, compared to 0.44 at *TSR* 4 for the taperless blade.

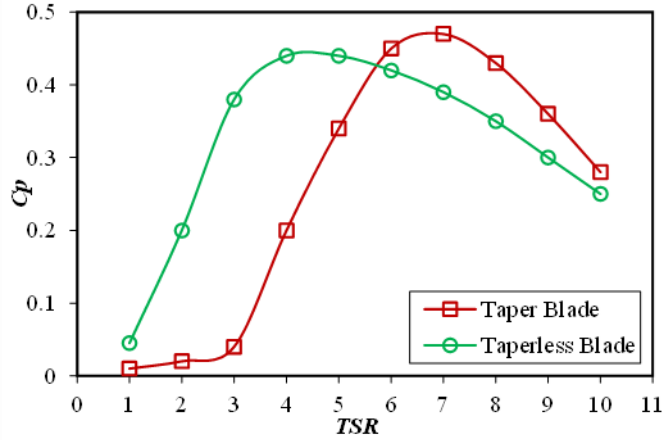


Figure 8. *TSR*- $C_p$ Curve of Taper and Taperless Blades

### 3.4. Comparison of Taper and Taperless Blade Electrical Power

Electric power ($P_l$) is obtained from the multiplication of system efficiency ($\eta_{sys}$) and wind power ($P_a$) according to Eq. 8, Wind power obtained from Eq. 6 is 3266.404 Watt, while system efficiency is derived from the multiplication of efficiency of blades, generator, controller, and transmission. Based on the calculation, the *Pl-TSR* curve is obtained, as shown in Figure 9. The red line curve is the result of the $C_p$ on the taper blade, while the green line is the result of the taperless blade. Both two $C_p$-*TSR* curves form the same graphic pattern. It is caused that the value of electric power is proportional to the coefficient of mechanical power. In the *TSR* 1 to 5, it can be seen that the green curve is above the red curve. On the contrary, it can be seen that the red curve is above the green curve in *TSR* 6 to 10. It means that the taperless blades show better electric power than the taper blades during the *TSR* 1 to 5. However, when in *TSR* 6 to 10 the taper blades show better electrical power than the taperless blades. So, the results show that the taper blades provide better electrical power than taperless at high wind speed conditions. In this case, it can be said that the taper blades are suitable for use as an ocean wind turbine design. For the taperless blade, it is not recommended for use in conditions of high wind speed because there is a stall which causes the electric power to decrease. Its application is suitable to be applied in low and moderate wind speed. As a result, taperless blades are not recommended for the design of ocean wind turbine.

Based on data from Figure 9, the Pl-TSR curve has shown that according to the design of the TSR 7, the taper blade produces the best electric power of 786 watts compared to the taperless of 652 watts. Pl max in taper blade is 786 watts on TSR 7, and the taperless blade is 736 watts on TSR 4.

The mechanical power and electrical power curves between two different blade types shown in Figure 10 have explained the power distribution produced by the taper blade (red line) and taperless blade (green line) blades. The results of this study have shown that taper blade is superior to taperless if viewed from the maximum mechanical and electrical power capacity. The results of the maximum mechanical and electrical power are 1535 watts and 786 watts for the taper blades and 1437 watts and 736 watts for the taperless blades, respectively.

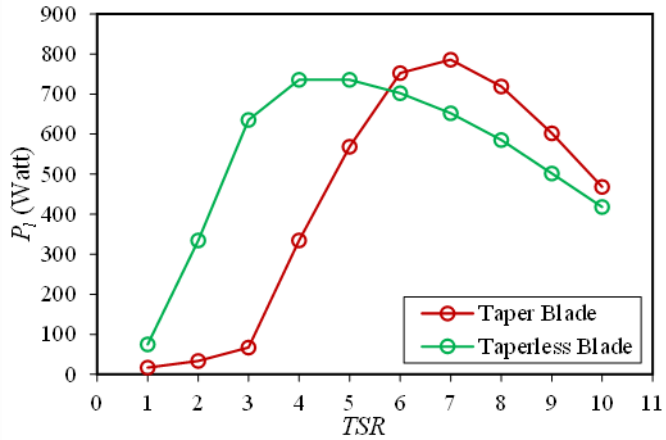


Figure 9. Electrical Power Curve of Taper and Taperless Blades

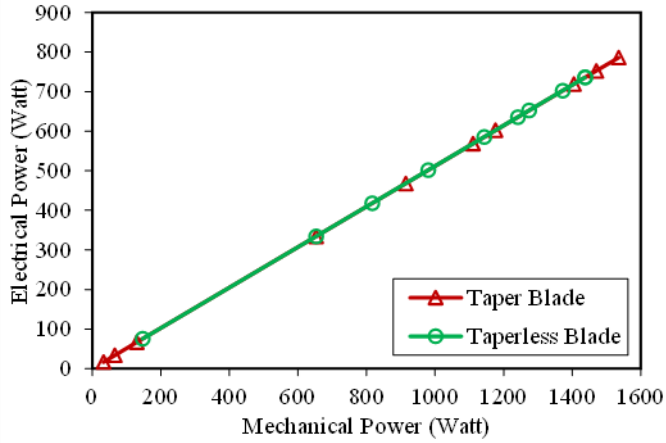


Figure 10. Electrical and Mechanical Power Curve of Taper and Taperless Blades

## 4. Conclusion

This research has been conducted in analyzing the comparison of taper blade and taperless blade applied for ocean wind turbine design. The obtained result shows that taper blades are highly recommended for use in ocean wind turbines compared to taperless blades. It is caused by the performance parameters such as power coefficient, mechanical power, and electrical power produced by taper blades is more significant than taperless blades at relatively high wind speeds. The maximum performance coefficient of power, mechanical power, and electrical power generated by the taper blades are, 0.47, 1535 watts, and 786 watts, respectively, while the respective taperless blades are, 0.44, 1437 watts, and 736 watts, respectively.

In further research, an advanced development study will be carried out using CFD to determine the fluid analysis that occurs around the taper and taperless blade. The final data generated from CFD can be used as a comparison of the previous data obtained from Q-Blade software. In the future, an experimental model using a laboratory-scale model to be tested can be performed so that the collected data is more realistic with the comparison of the results of Q-Blade and CFD.

## Acknowledgments

The authors wish to thank for the support from PT. Lentera Angin Nusantara who provided insight and service for design development and data.

## References

[1] Madi, M. E. N. Sasono, Y. S. Hadiwidodo and S. H. Sujiatanti, "Application of savonius turbine behind the propeller as energy source of fishing vessel in Indonesia," *IOP Conf. Series Materials Science and Engineering*, vol. 588, pp. 1-10, 2019. doi: 10.1088/1757-899X/588/1/012046

[2] M. J. Khan, G. Bhuyan, M. T. Iqbal and J. E. Quaicoe, "Hydrokinetic energy conversion systems and assesment of horizontal and vertical axis turbine for river and tidal aplications : A technology status review," *Applied Energy*, vol. 86, pp. 1823-1835, 2009. doi: 10.1016/j.apenergy.2009.02.017

[3] Md. J. Alam and M. T. Iqbal, "A low cut-in speed marine current turbine," Journal of Ocean Technology, vol 5, pp. 49-62, 2010.

[4] I. N. Zahrah, "Pengenalan teknologi pemanfaatan energi angin," Bahan Materi Pembelajaran, PT. Lentera Angin Nusantara, Indonesia, 2014.

[5] J. Wata, M. Faizal, B. Talu, L. Vanawalu, P. Sotia and M. R. Ahmed, "Studies on a low Reynolds number airfoil for small wind turbine applications," *Science China Technological Sciences*, vol. 54, no. 7, pp. 1684–1688, 2011. doi: 10.1007/s11431-011-4411-3

[6] L. Qiao, S. Wei, R. Gu, X. Quan, and Y. Yang, "The investigation of the airfoil for the small wind turbine based on the seagull airfoil," in *Asia-Pacific Power and Energy Engineering Conference (APPEEC)*, 2011. doi: 10.1109/APPEEC.2011.5748731

[7] S. M. Habali and I.A. Saleh, "Local design, testing and manufacturing of small mixed airfoil wind turbine blades of glassfiber reinforced plastics: part I: design ofthe blade and root," *Energy Conversion and Management*, vol. 41, no. 3, pp. 249–280, 2000. doi: 10.1016/S0196-8904(99)00103-X

[8] S. M. Habali and I.A. Saleh, "Local design, testing and manufacturing of small mixed airfoil wind turbine blades of glassfiber reinforced plastics: part II: manufacturing of the blade and rotor," *Energy Conversion and Management*, vol. 41, no. 3, pp. 281–298, 2000. doi: 10.1016/S0196-8904(99)00104-1

[9] K. Ameku, B. M. Nagai and J. N. Roy, "Design of a 3 kW windturbine generator with thin airfoil blades," *Experimental Thermal and Fluid Science*, vol. 32, no. 8, pp. 1723–1730, 2008. doi: 10.1016/j.expthermflusci.2008.06.008

[10] P. Giguere and M. S. Selig, "Low Reynolds number airfoils for small horizontal axis wind turbines," *Wind Engineering*, vol. 21, no. 6, pp. 367–380, 1997.

[11] R. K. Singh, M. R. Ahmed, M. A. Zullah and Y. H. Lee, "Design of a low Reynolds numberairfoil for small horizontal axis wind turbines," *Renewable Energy*, vol. 42, pp. 66–76, 2012. doi: 10.1016/j.renene.2011.09.014

[12] Y. Nishizawa, H. Tokuyama, Y. Nakajo and I. Ushiyama, "Yaw behavior of horizontal-axis small wind turbines in an urban area," *Wind Engineering*, vol. 33, no. 1, pp. 19–30, 2009. doi: 10.1260/0309-524X.33.1.19

[13] L. Mishnaevsky Jr, P. Freere, R. Sinha, P. Acharya, R. Shrestha and P. Manandhar, "Small wind turbines with timber blades for developing countries: materials choice, development, installation and experiences," *Renewable Energy*, vol. 36, no. 8, pp. 2128–2138, 2011. doi: 10.1016/j.renene.2011.01.034

[14] Q. Song and W. David Lubitz, "Design and testing of a new small wind turbine blade," *Journal of Solar Energy Engineering*, vol. 136, no. 3, 2014. doi: 10.1115/1.4026464

[15] Hasan, Md. Mehedi, A. El-Shahat and M. Rahman, "Design Studies and Aerodynamic Performance Analysis of Small Scale Horizontal Axis Wind Turbine Blade for Nano-Grid Applications," *Journal of Automation and Systems Engineering*, vol. 11, pp. 11-26, 2017.

[16] M. H. Lee, Y. C. Shiah and C. J. Bai, "Experiments and numerical simulations of the rotor-blade performance for a small-scale horizontal axis wind turbine," *Journal of Wind Engineering and Industrial Aerodynamics*, vol. 149, pp. 17–29, 2016. doi: 10.1016/j.jweia.2015.12.002

[17] F. Watanabe, T. Takahashi, H. Tokuyama, Y. Nishizawa and I. Ushiyama, "Modelling passive yawing motion of horizontal axis small wind turbine: derivation of new simplified equation for maximum yaw rate," *Wind Engineering*, vol. 36, no. 4, pp. 433–441, 2012. doi: 10.1260/0309-524X.36.4.433

[18] C. Mayer, M. E. Bechly, M. Hampsey, D. H. Wood, "The starting behaviour of a smallhorizontal-axis wind turbine," *Renewable Energy*, vol. 22, pp. 411–417, 2001. doi: 10.1016/S0960-1481(00)00066-5

[19] J. Yao, W. Yuan, J. Wang, J. Xie, H. Zhou, M. Peng, and Y. Sun, "Numerical simulation of aerodynamic performance for two dimensional wind turbine airfoils," *Procedia Engineering*, vol. 31, pp. 80–86, 2012. doi: 10.1016/j.proeng.2012.01.994

[20] P. A. C. Rocha, H. H. B. Rocha, F. O. M. Carneiro, M. E. Vieira da Silva and A. V. Bueno, "k–ω SST (shear stress transport) turbulence model calibration: A case study on a small scale horizontal axis wind turbine," *Energy*, vol. 65, pp. 412–418, 2014. doi: 10.1016/j.energy.2013.11.050

[21] A. El-Shahat, M. Hasan and A. Y. Abdelaziz, "Micro-Small-Scale Horizontal Axis Wind Turbine Design and Performance Analysis for Micro-Grids Applications," *Smart Microgrids*, pp. 65–117, 2019. doi: 10.1007/978-3-030-02656-1_6

[22] Madi, "Study of Horizontal Axis Wind Turbine Design with Different Airfoil Designs on Taper Blades for Sea Wind Power Plants at Ciheras Beach, PT. Lentera Angin Nusantara, (in Indonesian)" Job Training Report, Institut Teknologi Sepuluh Nopember, Indonesia, 2016.

[23] A. Effendi, M. Novriyanti, A. Y. Dewi and A. M. N. Putra,"Analisis pengaruh jumlah blade terhadap putaran turbin pada pemanfaatan energi angin di pantai ujung batu muaro penjalinan," Jurnal Teknik Elektro ITP, vol. 8, no.2, pp. 134-138, 2019.

[24] A. Bachtiar and W. Hayyatul, "Analisis potensi pembangkit listrik tenaga angin PT. Lentera Angin Nusantara (LAN) Ciheras," Jurnal Teknik Elektro ITP, vol. 7, no.1, pp. 35-45, 2018.

[25] I. N. Zahrah, "Dasar-dasar perancangan bilah," Bahan Materi Pembelajaran, PT.Lentera Angin Nusantara, Indonesia, 2014.